Opt Quant Electron (2016) 48:471
DOI 10.1007/s11082-016-0727-3

Analysis of efficiency limitations in high-power InGaN/GaN laser diodes

Joachim Piprek[1]

Received: 29 August 2016 / Accepted: 6 September 2016 / Published online: 27 September 2016
© Springer Science+Business Media New York 2016

Abstract Twenty years after their first demonstration by Shuji Nakamura, InGaN/GaN lasers still exhibit less than 40 % electrical-to-optical power conversion efficiency. This paper investigates reasons behind the efficiency limitation by advanced numerical simulations of measured high-power laser characteristics. Auger recombination is identified as a major limitation at all power levels, but the inherently high series resistance becomes the most restrictive limitation at higher power. Since the traditional efficiency analysis method produces misleading results, we propose an alternative method that is also applicable without numerical simulation.

Keywords Laser diode · InGaN/GaN · Efficiency · Auger recombination · Series resistance · Hole conductivity

1 Introduction

Shuji Nakamura predicted in his Nobel lecture that GaN-based laser diodes may replace light-emitting diodes (LEDs) in solid state lighting (SSL) applications (Nakamura 2014). InGaN/GaN lasers are already utilized in the headlights of some high-end cars. However, the main driving force behind most SSL applications is the promise of high energy efficiency. Some GaN-based blue LEDs achieve more than 80 % electrical-to-optical power conversion efficiency η_{PCE} (Hurni et al. 2015) but the highest η_{PCE} reported for GaN-based laser diodes is still below 40 % (Kawaguchi et al. 2016; Raring 2016). We here

This article is part of the Topical Collection on Numerical Simulation of Optoelectronic Devices 2016.

Guest edited by Yuh-Renn Wu, Weida Hu, Slawomir Sujecki, Silvano Donati, Matthias Auf der Maur and Mohamed Swillam.

✉ Joachim Piprek
piprek@nusod.org

[1] NUSOD Institute LLC, Newark, DE 19714-7204, US

investigate the reasons for the efficiency limitation of GaN-lasers by numerical analysis of measured high-power laser characteristics.

The power conversion efficiency η_{PCE} is defined as ratio of light output power P to electrical input power IU (I—current, U—bias). It can be separated into the electrical efficiency $\eta_U = h\nu/qU$ (hν—photon energy, q—electron charge) and the external quantum efficiency ($\eta_{PCE} = \eta_U \cdot \eta_{EQE}$). The latter is the ratio of emitted photon number to injected number of electron–hole pairs. It is typically split up (Crump et al. 2013) into a current-averaged differential slope efficiency $\eta_S = P(q/h\nu)/(I - I_{th})$ and the threshold current efficiency $\eta_{th} = (I - I_{th})/I$ (I_{th}—threshold current, $\eta_{EQE} = \eta_S \cdot \eta_{th}$). Note that η_S is unitless and differs from the common slope efficiency $P/(I - I_{th})$ given in W/A as well as from the differential efficiency dP/dI, especially with sub-linear P(I). It is also important to point out that the threshold current is considered constant in this model. Our analysis will show that such approach delivers misleading results if the laser experiences relevant self-heating. Rising temperatures reduce the optical gain and cause the threshold carrier density as well as the threshold current to grow with higher current. We propose an alternative approach which is also applicable without any simulation.

2 Models and parameters

The numerical laser model is based on the LASTIP simulation software (Crosslight 2015). It self-consistently computes carrier transport, the wurtzite electron band structure of strained InGaN quantum wells (QWs), stimulated photon emission, wave guiding, and heat flow. Schrödinger and Poisson equations are solved iteratively in order to account for the QW deformation with changing device bias (quantum-confined Stark effect). The transport model includes drift and diffusion of electrons and holes, Fermi statistics, built-in polarization and thermionic emission at hetero-interfaces, as well as all relevant radiative and non-radiative recombination mechanisms. More details on the employed laser models can be found elsewhere (Piprek 2003).

Our analysis focuses on recently published experimental results for 405 nm GaN-based Fabry–Perot laser diodes exhibiting a light output power of P = 7.2 W at I = 4 A input current and U = 6.3 V bias in continuous-wave (CW) operation at room temperature (Kawaguchi et al. 2016). The authors claim that this is the highest power among single-stripe InGaN/GaN laser diodes reported thus far. It is based on an optimized ridge-waveguide structure with low modal loss ($\alpha_i = 2$/cm) as well as on a low thermal resistance of about 6 K/W (Nozaki et al. 2016). The ridge is 12 μm wide and the cavity is 1200 μm long. Facet reflectivities are 0.056 and 0.95, respectively.

Vertical waveguide structure and lasing mode are illustrated in Fig. 1. The low modal loss was accomplished by using thick undoped GaN waveguide layers which reduce the modal overlap with the highly absorptive p-doped layers. The p-$Al_{0.36}GaN$ electron blocking layer (EBL) was moved to the p-side edge of the waveguide in order to minimize the bias (Kawaguchi et al. 2016). The $In_{0.066}GaN/In_{0.008}GaN$ multi-quantum well (MQW) active region features 7.5 nm thick quantum wells with an optical confinement factor of 3.8 %. MQW energy band diagram and quantum levels are shown in Fig. 2 and demonstrate the deformation by the built-in polarization which separates electrons and holes and which is still not fully screened despite the high injection current density of 28 kA/cm^2.

Key material parameters are obtained by simulating the measured laser performance (Fig. 3). The threshold current is reproduced by using QW Auger coefficients of

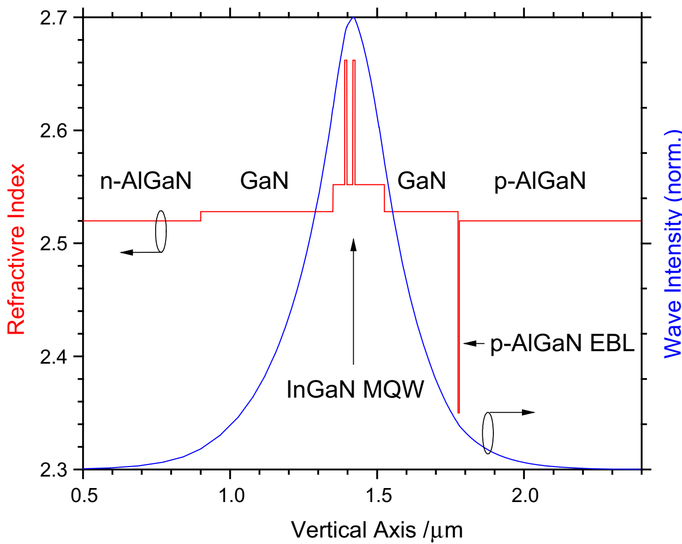

Fig. 1 Vertical profiles of the refractive index and the simulated lasing mode (normalized, MQW—multi-quantum well, EBL—electron blocking layer)

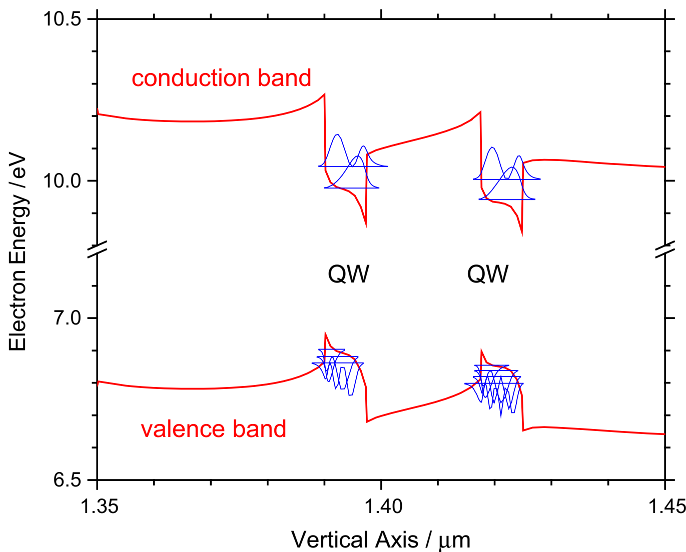

Fig. 2 Energy band diagram of the two InGaN/GaN quantum wells (QW) with quantum level wave functions (*blue*) as calculated for the reference laser structure at I = 4A. (Color figure online)

$C_n = 65 \times 10^{-31}$ cm^6/s and $C_p = 6 \times 10^{-31}$ cm^6/s at room temperature. This large C_n/C_p ratio is in agreement with recent measurements which find ratios of up to 12 (Nirschl et al. 2016). Theoretical QW Auger coefficients for the dominating indirect transitions have not been published yet, but calculations for bulk InGaN also suggest a large ratio C_n/C_p (Bertazzi et al. 2012). Implementation of the reported modal loss $\alpha_i = 2$/cm gives good

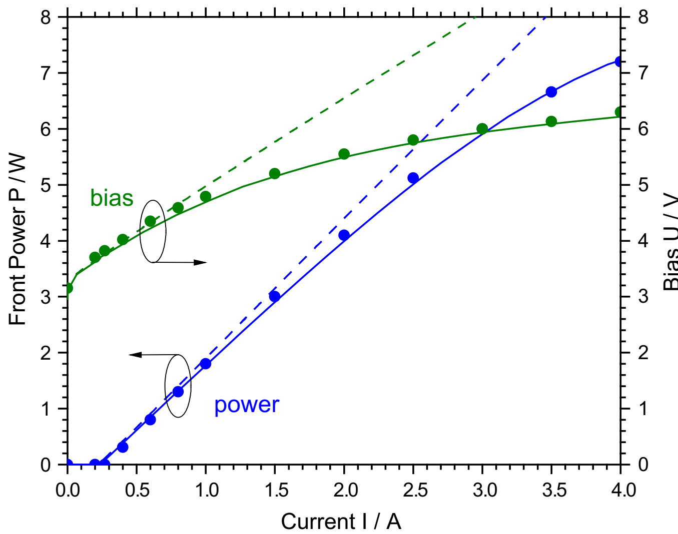

Fig. 3 Comparison between measurements (*dots*) and simulations (*lines*). The *dashed lines* are simulated without self-heating

agreement with the measured P(I) characteristic. Our simulation also reproduces the injection efficiency of $\eta_i = 92\ \%$ measured in pulsed operation without self-heating (Kawaguchi et al. 2016). The calculated MQW temperature rise in CW operation is $\Delta T = 110$ K at I = 4A corresponding to a thermal resistance of $\Delta T/(IU-P) = 6$ K/W as measured (Nozaki et al. 2016). For comparison, Fig. 3 also shows simulation results without self-heating (dashed lines). The P(I) sub-linearity in CW operation is obviously caused by the temperature rise which reduces the QW gain and therefore requires an increasing QW threshold carrier density (Piprek and Nakamura, 2002). This leads to enhanced QW Auger recombination which is the dominating carrier loss mechanism in our case (see below).

The bias-current simulations shown in Fig. 3 with and without self-heating reveal a thermal reduction of the series resistance. This phenomenon was also observed experimentally (Raring et al. 2010; Becerra et al. 2015) and it is mainly caused by the thermal activation of holes in the p-$Al_{0.026}GaN$ cladding layer (Piprek 2015). The Mg acceptor ionization energy is 178 meV in that layer and the acceptor density was calibrated to match the reported density of 10^{18} cm^{-3} free holes (Kawaguchi et al. 2016). Hole mobility ($\mu_p = 2$ cm^2/Vs) and contact resistivity ($R_c = 0.05$ mΩ cm^2) were then adjusted to achieve agreement with the bias measurement in Fig. 3. Both numbers are not reported for this laser but quite reasonable (Yonkee et al. 2016).

3 Analysis and discussion

Figure 4 plots the current fractions consumed by different physical mechanisms inside the laser. Stimulated emission starts at the initial threshold current of $I_{th} = 227$ mA which is mainly controlled by QW Auger recombination and by spontaneous photon emission. Leakage current is negligible at that point and so is the Shockley–Read–Hall (SRH)

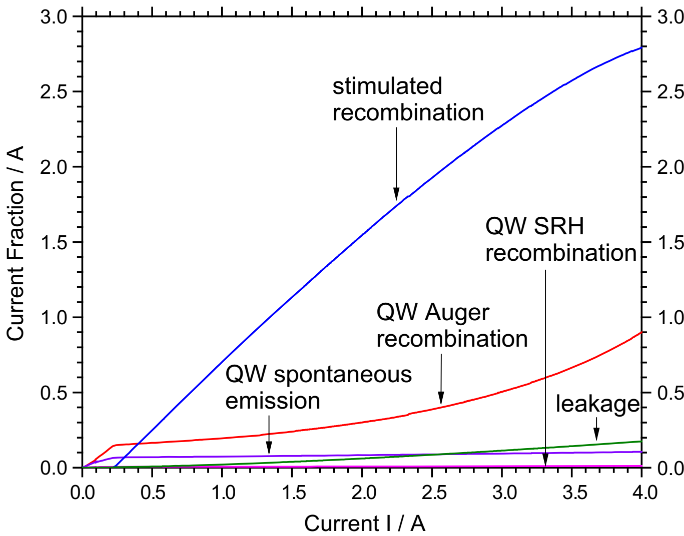

Fig. 4 Simulated fractions of the total injection current as consumed by different recombination mechanisms. Recombination outside the quantum wells (QWs) is considered leakage

recombination, despite the relatively short SRH carrier lifetime of 20 ns assumed for the QWs. Even at high current, the latter remains irrelevant. Electron leakage into the p-side waveguide layer rises to about 4 % of the total current while QW Auger recombination consumes 22 % of all carriers at I = 4 A. Adding up all these contributions leads to a threshold current $I_{th}(I) = 1.2$ A at I = 4 A. The increase in threshold current is responsible for the P(I) sub-linearity in Fig. 3 since the optical loss is considered temperature independent. Carrier leakage from the waveguide layers remains negligible.

Our efficiency analysis applies the separation $\eta_{PCE} = \eta_U \cdot \eta_{th} \cdot \eta_S$ as outlined in the introduction. However, in contrast to the typical assumption of a fixed threshold current I_{th} and a fixed photon energy hν, we here include the simulated changes $I_{th}(I)$ and hν(I) with rising MQW temperature. The results are plotted as solid lines in Fig. 5. The slope efficiency η_S is the least limiting mechanism in the reference laser, based on the record-low optical loss. The threshold efficiency η_{th} is dominated by QW Auger recombination and it limits the PCE more strongly, especially at low power. But at higher power, the declining electrical efficiency η_U becomes the most restrictive factor. This is mainly attributed to the poor hole conductivity in the p-cladding layer which is related to the large ionization energy of Mg acceptors. The required high Mg density not only reduces the hole mobility by scattering but also contributes to photon losses by band-tail absorption (Piprek et al. 2007). The photon-energy dependent relationship between Mg density and absorption has not been clearly identified (Kioupakis et al. 2010) so that it is difficult to find the ideal balance between hole conductivity and optical loss theoretically. Several alternative p-side cladding concepts are currently explored, such as indium-tin-oxide cladding layers (Pourhashemi et al. 2015) and tunnel-junctions (Yonkee et al. 2016).

For comparison, Fig. 5 also shows the results with fixed $I_{th} = 227$ mA and hν = 3.066 eV as dashed lines. The calculated red-shift hν(I) turns out to have a negligible influence on the electrical efficiency $\eta_U = = h\nu/qU$ since QW bandgap shrinkage and band filling effects almost compensate each other. The slope efficiency $\eta_S \propto P/(I-Ith)$ is

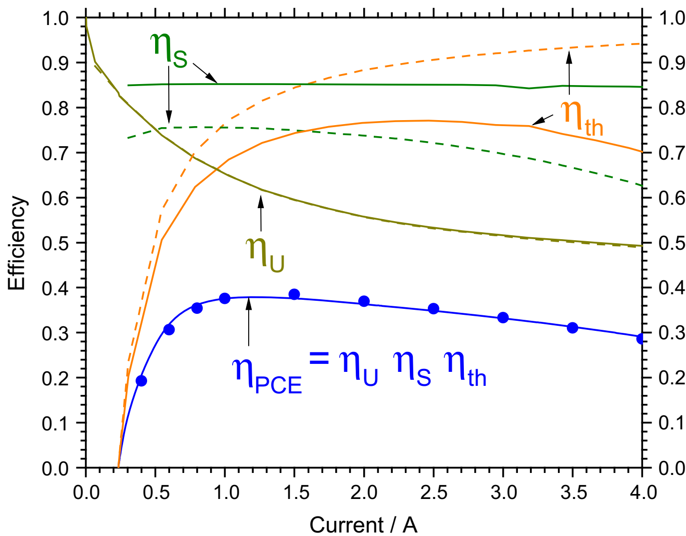

Fig. 5 Efficiency versus current: η_{PCE}—power conversion efficiency (dots from measurements), η_U—electrical efficiency, η_{th}—threshold current efficiency, η_S—slope efficiency (*solid/dashed*: with/without temperature sensitivity of threshold current and emission wavelength)

always larger with rising threshold current than with fixed threshold current. But most importantly, the significant difference between solid and dashed lines for $\eta_{th}(I)$ demonstrates that the thermally induced change in threshold current $I_{th}(I)$ should not be neglected. An approximate function $I_{th}(I)$ can be directly extracted from the measurement by keeping the slope efficiency constant at the threshold value, i.e., by shifting the dashed blue line in Fig. 3 parallel to the current axis so that a value $I_{th}(P)$ can be assigned to every power P(I) in CW operation. However, the change in threshold current is smaller if the self-heating leads to increased absorption (Piprek et al. 2000). Thus, the solid and dashed lines in Fig. 5 represent the two extreme cases of constant slope efficiency and constant threshold current, respectively.

Figure 6 demonstrates the effect of excluding efficiency limiting mechanisms from the simulation. The separation of electrons and holes shown in Fig. 2 is reduced by eliminating the built-in polarization and it raises the peak efficiency to 46 % (purple curve). As expected from Fig. 5, the optical loss of $\alpha_i = 2$/cm is already very low and its complete elimination only increases the peak efficiency to 48 % (green curve) since the QW threshold carrier density is slightly lower and therefore also the Auger recombination. Without QW Auger recombination, the threshold current drops significantly and hardly changes with increasing current, so that η_{PCE} peaks at 67 % (red curve). But the bias remains almost unchanged and drives the efficiency below 40 % at high power. Some bias reduction can be achieved by eliminating the small contact resistance R_c but this only raises the peak power conversion efficiency to 43 % (orange curve). Finally, we simulate the effect of an alternative p-cladding layer with 50-times higher hole mobility of $\mu_p = 100$ cm^2/Vs (dark yellow curve, $R_c = 0$). The efficiency is significantly enhanced up to 57 % and remains near this peak value even with rising current, while all other simulated exclusions are unable to surpass the apparently magic number of $\eta_{PCE} = 40$ % at high power.

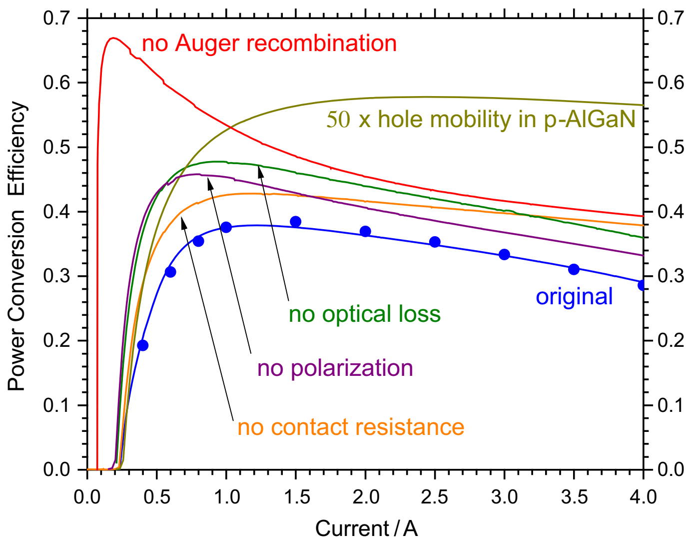

Fig. 6 Power conversion efficiency versus current for various parameter variations as discussed in the text (*dots* from measurements)

4 Summary

In summary, we identified the poor hole conductivity of the Mg doped cladding layer as main reason for the low energy conversion efficiency of high-power InGaN/GaN lasers. However, restrictions due to increasing Auger recombination cannot be neglected. We proposed an improved efficiency analysis of laser diodes by considering the thermally induced rise of the threshold current.

References

Becerra, D.L., Kuritzky, L.Y., Nedy, J., Saud Abbas, A., et al.: Measurement and analysis of internal loss and injection efficiency for continuous-wave blue semipolar (2021) III-nitride laser diodes with chemically assisted ion beam etched facets. Appl. Phys. Lett. **108**, 091106 (2015)

Bertazzi, F., Goano, M., Bellotti, E.: Numerical analysis of indirect Auger transitions in InGaN. Appl. Phys. Lett. **101**, 011111 (2012)

Crosslight Software Inc., Vancouver, Canada (2015)

Crump, P., Erbert, G., Wenzel, H., Frevert, C., et al.: Efficient high-power laser diodes. J. Sel. Top. Quantum Electron. **19**, 1501211 (2013)

Hurni, C.A., David, A., Cich, M.J., Aldaz, R.I., et al.: Bulk GaN flip-chip violet light-emitting diodes with optimized efficiency for high-power operation. Appl. Phys. Lett. **106**, 031101 (2015)

Kawaguchi, M., Imafuji, O., Nozaki, S., Hagino, H., et al.: Optical-loss suppressed InGaN laser diodes using undoped thick waveguide structure. Proc. SPIE **9748**, 974818 (2016)

Kioupakis, E., Rinke, P., Van de Walle, C.: Determination of internal loss in nitride lasers from first principles. App. Phys. Express **3**, 082101 (2010)

Nakamura, S.: Nobel lecture (2014). https://www.nobelprize.org/nobel_prizes/physics/laureates/2014/nakamura-lecture.html (2014)

Nirschl, A., Binder, M., Schmid, M., Pietzonka, I., et al.: Towards quantification of the crucial impact of auger recombination for the efficiency droop in (AlInGa)N quantum well structures. Opt. Express **24**, 2971–2980 (2016)

Nozaki, S.,Yoshida, S., Yamanaka, K., Imafuji, O. et al.: High-power and high-temperature operation of an InGaN laser over 3 W at 85°C using a novel double-heat-flow packaging technology. Jpn. J. Appl. Phys. **55**, 04EH05 (2016)

Piprek, J.: Semiconductor Optoelectronic Devices: Introduction to Physics and Simulation. Academic Press, San Diego (2003)

Piprek, J., Abraham, P., Bowers, J.E.: Self-Consistent Analysis of High-Temperature Effects on Strained-Layer Multi-Quantum Well InGaAsP/InP Lasers. IEEE J.Quantum Electron. **36**, 366–374 (2000)

Piprek, J., Nakamura, S.: Physics of High-Power InGaN/GaN Lasers. IEE Proc. Optoelectr. **149**, 145–151 (2002)

Piprek, J., Wenzel, H., Kneissl, M.: Analysis of wavelength-dependent performance variations of GaN-based ultraviolet lasers. Proc. SPIE **6766**, 67660H (2007)

Piprek, J.: How to decide between competing efficiency droop models for GaN-based light-emitting diodes. Appl. Phys. Lett. **107**, 031101 (2015)

Pourhashemi, A., Farrell, R., Cohen, D., Speck, J., et al.: High-power blue laser diodes with indium tin oxide cladding on semipolar (2021) GaN substrates. Appl. Phys. Lett. **106**, 111105 (2015)

Raring, J., Schmidt, M.C., Poblenz, C., Chang, Y., et al.: High-Efficiency Blue and True-Green-Emitting Laser Diodes Based on Non-*c*-Plane Oriented GaN Substrates. Appl. Phys. Expr. **3**, 112101 (2010)

Raring, J.W.: Laser diodes for next generation light sources. DOE SSL R&D Workshop, Raleigh (2016)

Yonkee, B.P., Young, E.C., Lee, C., Leonard, J.T., et al.: Demonstration of a III-nitride edge-emitting laser diode utilizing a GaN tunnel junction contact. Opt. Express **24**, 7816–7822 (2016)